10.1098/rsta.2004.1454

THE ROYAL SOCIETY

Raman spectroscopy of graphite

By Stephanie Reich[1] and Christian Thomsen[2]

[1]*Department of Engineering, University of Cambridge, Trumpington Street, Cambridge CB2 1PZ, UK* (sr379@eng.cam.ac.uk)
[2]*Institut für Festkörperphysik, Technische Universität Berlin, Hardenbergstr. 36, 10623 Berlin, Germany*

Published online 14 September 2004

We present a review of the Raman spectra of graphite from an experimental and theoretical point of view. The disorder-induced Raman bands in this material have been a puzzling Raman problem for almost 30 years. Double-resonant Raman scattering explains their origin as well as the excitation-energy dependence, the overtone spectrum and the difference between Stokes and anti-Stokes scattering. We develop the symmetry-imposed selection rules for double-resonant Raman scattering in graphite and point out misassignments in previously published works. An excellent agreement is found between the graphite phonon dispersion from double-resonant Raman scattering and other experimental methods.

Keywords: Raman scattering; graphite; phonon dispersion; double-resonant scattering; symmetry

1. Introduction

Graphite is one of the longest-known forms of pure carbon and familiar from everyday life. It is built from hexagonal planes of carbon atoms. In ideal graphite these planes are stacked in an ABAB manner. Macroscopic single crystals of graphite do not occur in nature. So-called kish graphite—which is often referred to as a single crystal—consists of many small crystallites (up to $100\times100\,\mu m^2$) which are oriented randomly. Highly oriented pyrolytic graphite (HOPG) is artificially grown graphite with an almost perfect alignment perpendicular to the carbon planes. Along the in-plane directions, however, the crystallites are again small and randomly oriented. The disorder in a graphite sample gives rise to a number of Raman peaks with quite peculiar properties (Tuinstra & Koenig 1970). Vidano *et al.* (1981) found that the disorder-induced Raman modes depend on the energy of the incoming laser light; their frequencies shift when the laser energy is changed. This puzzling behaviour was shown by Thomsen & Reich (2000) to originate from a double-resonant Raman process close to the K point of the graphite Brillouin zone. For a given incoming laser energy, the double-resonant condition selectively enhances a particular phonon wave vector; the corresponding frequency is then observed experimentally.

Double resonances also explain the frequency difference between Stokes and anti-Stokes scattering in graphite (Tan *et al.* 1998). Particularly interesting is that the

One contribution of 13 to a Theme 'Raman spectroscopy in carbons: from nanotubes to diamond'.

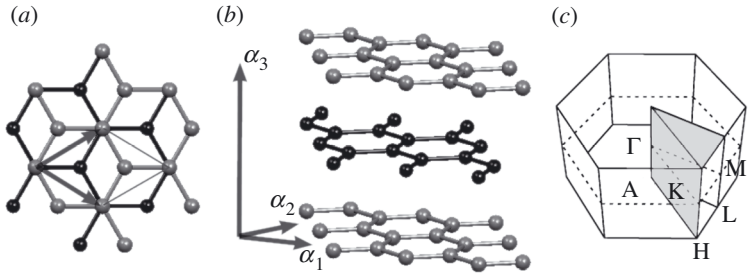

Figure 1. Graphite lattice in (*a*) top and (*b*) side view. $\boldsymbol{a}_1$, $\boldsymbol{a}_2$ and $\boldsymbol{a}_3$ span the unit cell of graphite. (*c*) Brillouin zone of graphite. The irreducible domain is spanned by the Γ–M–K–Γ triangle within the plane. Γ–A is the direction corresponding to the $\boldsymbol{a}_3$ lattice vector in reciprocal space.

phonon wave vectors giving rise to the disorder-induced Raman bands are large compared with the extension of the Brillouin zone (Thomsen & Reich 2000). Thus, Raman scattering can be used to measure the phonon dispersion for wave vectors normally reserved to neutron or inelastic X-ray scattering, which was first pointed out by Saito *et al.* (2002). The concept of double-resonant Raman scattering has been applied to other sp^2 bonded carbon systems, most notably carbon nanotubes, during the last three years. These topics are reviewed in other articles in this issue and will not be considered here. An alternative model for the Raman spectrum of graphite is based on small aromatic molecules; it was suggested by Castiglioni *et al.* (2001) and is discussed likewise in another article of this issue.

In this paper we review the vibrational properties of graphite as measured by Raman spectroscopy. We first consider the symmetry of graphite, its phonon branches and Raman selection rules in § 2. Section 3 introduces the Raman spectra of graphite with emphasis on the disorder-induced modes and their overtones in the second-order spectrum. In particular, we describe the three key experiments that established the unusual properties of the disorder-induced bands experimentally. The theory of double-resonant Raman scattering is developed in § 4. We begin with the examples of two linear electronic bands, where the Raman cross-section can be calculated analytically. We then apply double-resonant Raman scattering to graphite and show that the peculiar excitation-energy dependence follows naturally from the double-resonant condition. The rest of § 4 treats the selection rules for double-resonant scattering, and the second-order and the anti-Stokes Raman spectra. Finally, we show in § 5 how to obtain the phonon dispersion from the disorder-induced and second-order Raman peaks in graphite. Section 6 summarizes this work.

2. Symmetry and selection rules

Graphite is built from hexagonal planes of carbon atoms; it contains four atoms in the unit cell (see figure 1). The two planes are connected by a translation $\boldsymbol{t} = (\boldsymbol{a}_1 + \boldsymbol{a}_2)/3 + \boldsymbol{a}_3/2$ or by a C_6 rotation about the sixfold symmetry axis followed by a translation $\boldsymbol{a}_3/2$ ($\boldsymbol{a}_i$ are the graphite lattice vectors (see figure 1)). Graphite belongs to the $P6_3/mmc$ (D^4_{6h}) space group; its isogonal point group is D_{6h}. When studying the physical properties of graphite it is often sufficient to consider only a single hexagonal plane of carbon atoms (graphene), because the interaction between

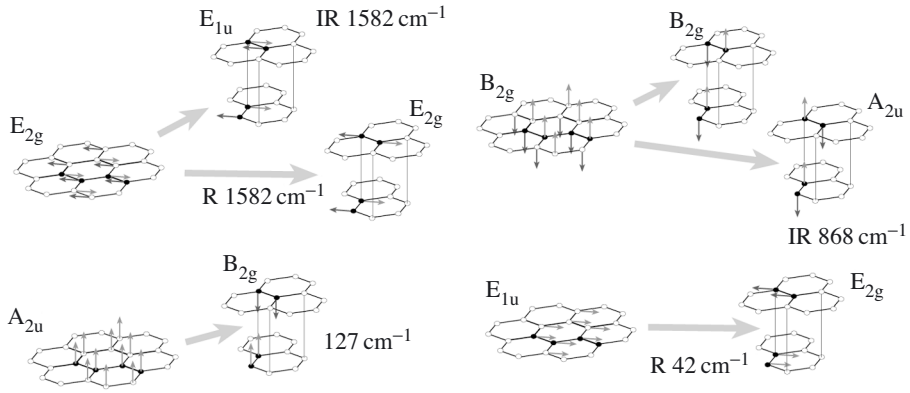

Figure 2. Phonon eigenvectors of graphene and graphite. Every phonon eigenvector of graphene gives rise to two vibrations of graphite. For example, the in-phase combination of the two layers for the E_{2g} optical mode of graphene yields $E_{2g} \otimes A_{1g} = E_{2g}$ and the out-of-phase combination $E_{2g} \otimes B_{1u} = E_{1u}$. Next to the graphite modes we indicate whether they are Raman (R) or infrared (IR) active and the experimentally observed phonon frequencies. The translations of graphite were omitted from the figure.

the layers is very weak. However, even a weak interaction can change selection rules in a crystal. We therefore first derive the normal modes of graphene; we then look at how their symmetries are affected by stacking the planes.

Graphene has six normal modes at $q = 0$, which can be found by standard procedures (Rousseau *et al.* 1981; Wilson *et al.* 1980; Yu & Cardona 1996):

$$\Gamma_{\mathrm{vib,2D}} = \mathrm{A_{2u}} \oplus \mathrm{B_{2g}} \oplus \mathrm{E_{1u}} \oplus \mathrm{E_{2g}}. \tag{2.1}$$

The A_{2u} and E_{1u} representations are the translations of the plane; the B_{1g} mode is an optical phonon where the carbon atoms move perpendicular to the graphene planes. Finally, E_{2g} is the doubly degenerate in-plane optical vibration. Only the E_{2g} representation is Raman active.

The normal modes of graphene can be combined either in phase ($\Gamma_{\mathrm{vib,2D}} \otimes \mathrm{A_{1g}}$) or out of phase ($\otimes \mathrm{B_{1u}}$) to obtain the vibrations of graphite.† From the vibrational representation of graphene $\Gamma_{\mathrm{vib,2D}}$ we thus find the phonon symmetries of graphite:

$$\Gamma_{\mathrm{vib,3D}} = 2\mathrm{A_{2u}} \oplus 2\mathrm{B_{2g}} \oplus 2\mathrm{E_{1u}} \oplus 2\mathrm{E_{2g}}. \tag{2.2}$$

Figure 2 illustrates how the graphene modes split into a higher-frequency out-of-phase and a lower-frequency in-phase vibration. The in-phase combination of a Raman-active phonon of graphene is also Raman active in graphite, the out-of-phase combination never. On the other hand, the out-of-phase combination of a phonon eigenvector that is not Raman active for the single plane might or might not be Raman active in the graphite crystal (see, for example, the E_{2g} and B_{2g} low-energy modes in figure 2). A graphite crystal thus has two Raman-active vibrations at the Γ point of the Brillouin zone. The high-energy E_{2g} phonon is constructed from the

† The terms 'in phase' and 'out of phase' refer to the atoms in the two planes that are connected by, for example, the inversion or the diagonal glide planes. The two carbon atoms on top of each other in figure 1*a* at $(0, 0, 0)$ and $(0, 0, \frac{1}{2})$ move in opposite directions in the in-phase combination of the two planes.

in-plane optical mode of graphene; in the low-energy E_{2g} mode the graphene planes slide against each other.

We will see in the following sections that the Raman spectrum of graphite involves phonons which are non-Γ-point vibrations. When going away from $q = 0$ along one of the in-plane high-symmetry directions Γ–M (Σ) and Γ–K–M (T) the point group symmetry is reduced to C_{2v}. Both the in-plane optical and acoustic phonons thereby split into two non-degenerate modes which belong to A_1 and B_1 in the molecular notation. More precisely, the LO and LA phonons transform according to Σ_1, the TO and TA according to Σ_3 along Γ–M; along Γ–K–M the TO and LA branches belong to T_1 and the LO and TA branches to T_3. At the high-symmetry points M and K of the in-plane section of the Brillouin zone, we have

$$\Gamma_{\mathrm{vib,M,2D}} = \mathrm{M}_1^+ \oplus \mathrm{M}_2^+ \oplus \mathrm{M}_2^- \oplus \mathrm{M}_3^+ \oplus \mathrm{M}_3^- \oplus \mathrm{M}_4^- \tag{2.3}$$

and

$$\Gamma_{\mathrm{vib,K,2D}} = \mathrm{K}_1 \oplus \mathrm{K}_2 \oplus \mathrm{K}_5 \oplus \mathrm{K}_6. \tag{2.4}$$

Note that at all high-symmetry points, Γ, M and K, the phonon eigenvectors of graphene are completely given by symmetry (see Mapelli *et al.* 1999). Considering that the eigenvectors are known at the most important parts of the Brillouin zone, it is quite surprising that the published phonon dispersions differ strongly in the calculated phonon frequencies and shapes, in particular, of the optical branches (Dubay & Kresse 2003; Grüneis *et al.* 2002; Jishi & Dresselhaus 1982; Mapelli *et al.* 1999; Maultzsch *et al.* 2004; Pavone *et al.* 1993; Sánchez-Portal *et al.* 1999). It can be shown that the differences arise mainly from the assignment of the M-point eigenvectors to the phonon branches of graphite. For example, Mapelli *et al.* (1999) and Kresse *et al.* (1995) assigned the LA mode to the totally symmetric vibration at M, whereas Pavone *et al.* (1993), Sánchez-Portal *et al.* (1999) and Dubay & Kresse (2003) found the M-point LO mode to be totally symmetric. These discrepancies were resolved recently by inelastic X-ray measurements of the graphite phonon dispersion performed by Maultzsch *et al.* (2004). The phonon dispersion is further discussed in § 5 of this paper (see, in particular, figure 9).

3. Raman spectrum of graphite

Figure 3*a* shows the Raman spectrum of graphite that is observed on well-ordered defect-free samples (Nemanich & Solin 1979; Tuinstra & Koenig 1970; Wang *et al.* 1990). The first-order spectrum shows the E_{2g} optical mode at 1583 cm^{-1}. The intensity of this peak is independent of the polarization in the Raman experiment as expected for an E_{2g} Raman tensor (Cardona 1982). The second-order spectrum of graphite is quite remarkable in several aspects. The frequency of the G^* peak is greater than the E_{2g} frequency (indicated by the vertical dotted line in figure 3*a*). The G^* peak is associated with the overbending of the longitudinal optical branches of graphite, i.e. the LO branch has its maximum away from the Γ point of the Brillouin zone in contrast to most other materials. Secondly, it is apparent in figure 3*a* that the second-order spectrum is very strong when compared with the first-order peak. The most intense D^* line, moreover, is clearly not an overtone of a Raman-allowed first-order phonon. While second-order scattering by overtones of non-Raman-active vibrations is, in general, allowed in graphite, their intensities are expected to be weak compared with the first-order Raman spectrum.

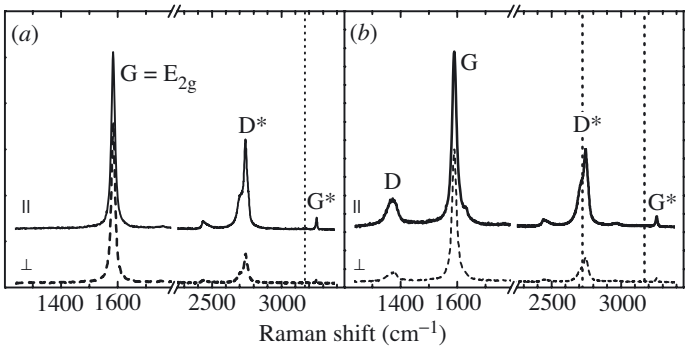

Figure 3. The Raman spectrum of graphite. The spectra were measured on different spots of kish graphite. (*a*) First- and second-order Raman spectrum of a perfect crystallite in the sample. The first-order spectrum shows a single line at 1583 cm^{-1}. Note the high intensity of the second-order spectrum. (*b*) Raman spectrum of graphite in the presence of disorder in the focal spot of the laser. An additional line at 1370 cm^{-1} and a high-energy shoulder at the E_{2g} line are observed. The spectra in (*a*) and (*b*) were corrected for the sensitivity of the Raman set-up. Full (dashed) lines are for parallel (crossed) polarization of the incoming and outgoing light; the spectra in parallel polarization were shifted for clarity. The dotted lines are positioned at twice the frequency of the fundamentals of the D and G modes.

The situation gets even more interesting when we collect the Raman scattered light on a disordered part of the sample as in figure 3*b* (Tuinstra & Koenig 1970). The intensity ratio of the E_{2g} line in crossed (dashed line) and parallel (full) polarization is $I_\perp/I_\parallel \sim \frac{3}{4}$, ensuring that the graphite crystallites are small and randomly oriented in the area of the laser spot (Cardona 1982; Wilson *et al.* 1980). At *ca.* 1370 cm^{-1} a new line appears in the Raman spectrum, which was first reported by Tuinstra & Koenig (1970), and named D mode for disorder-induced mode. The second-order spectrum is less affected by disorder. Nevertheless, it now becomes apparent that the D^* feature is very close to twice the D mode energy. It is tempting to assign the D^* mode to an overtone of the D band, and we will later see that this is indeed the case.

The D, D^* and G^* modes were known experimentally for three decades before their origin and their peculiar behaviour were explained theoretically (Thomsen & Reich 2000).† Let us briefly review the three key experiments that established the properties of the graphite Raman spectra. Tuinstra & Koenig (1970) showed that the intensity of the D band compared with the Raman-allowed E_{2g} mode depends on the size of the graphite microcrystals in the sample (see figure 4*a*). Wang *et al.* (1990) generalized the intensity dependence to any kind of disorder or defects in the sample by recording the D mode intensity on boron-doped and electrochemically oxidized HOPG. Boron doping is substitutional in graphite; the crystallites in HOPG thus remain comparatively large. Nevertheless, the symmetry breaking by the boron

† In the early literature on Raman scattering, in graphite the E_{2g} mode at 1580 cm^{-1} was usually called the G peak and the overtone of the D mode, i.e. the D^* peak, was called the G' peak. The Raman peaks at *ca.* 1350, 1620 and 3250 cm^{-1} were referred to as D, D' and D''. This convention arose because the G and D^* appear with strong intensity on perfect graphite crystals and were labelled G for graphite. The other modes are either observed only on defective samples or are very weak in intensity like the G^* peak that was incorrectly assigned as a defect-induced feature. In this paper we use the modern convention, where D stands for modes coming approximately from the K point of graphite and G for vibrations close to the Γ point; additionally, overtones are denoted by an asterisk.

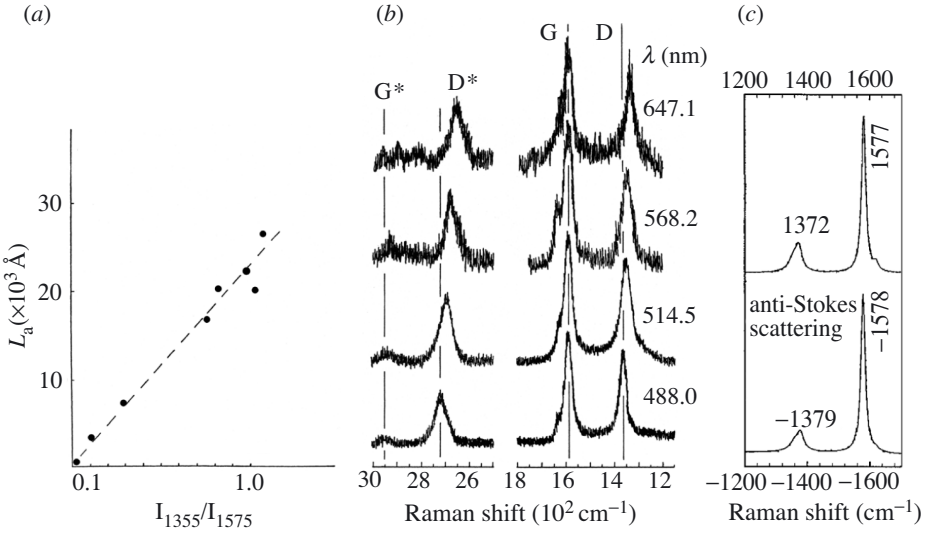

Figure 4. (*a*) Dependence of the relative D mode intensity on the length-scale L_a of the graphite microcrystallites (after Tuinstra & Koenig 1970). (*b*) Excitation-energy dependence of the first- and second-order Raman spectra of graphite (after Vidano *et al.* 1981). (*c*) Stokes (top) and anti-Stokes (bottom) Raman scattering of the D and E_{2g} modes in graphite (after Tan *et al.* 1998).

atoms gives rise to a strong D band. This mode thus appears regardless of the type of disorder.

The truly puzzling piece of information was added by Vidano *et al.* (1981) by Raman scattering on graphite employing different excitation energies. Figure 4*b* reproduces their spectra recorded between 1.91 and 2.53 eV (647–488 nm). The frequency of the D mode shifts to higher energies with increasing excitation energy. The shift was observed to be linear over a wide range of excitation energies (near IR to near ultraviolet (UV)) with a slope between 40 and 50 cm^{-1} eV^{-1} (Matthews *et al.* 1999; Pócsik *et al.* 1998; Vidano *et al.* 1981; Wang *et al.* 1990). The D* band has twice the slope of the D band, confirming the assignment as an overtone that we mentioned above. Subsequently, many other much weaker Raman modes were also reported to have laser-energy-dependent frequencies in graphite (Kawashima & Katagiri 1995; Tan *et al.* 2001); a similar behaviour is also observed in other carbon materials (Ferrari & Robertson 2001; Maultzsch *et al.* 2003). Finally, Tan *et al.* (1998) observed that the Stokes frequencies of the D, D* and other modes differ from the respective anti-Stokes frequencies (see figure 4*c* for the D mode range). All these observations apparently contradict our fundamental understanding of Raman scattering. We will see in the following that the excitation-energy dependence of the phonon frequencies and other effects arise from a double resonance peculiar to the electronic band structure of graphite and other sp^2 bonded carbon materials.

4. Double-resonant Raman scattering

The first attempts to explain the appearance of disorder modes in graphite suggested, among other mechanisms, Raman-forbidden Γ-point vibrations activated by disorder

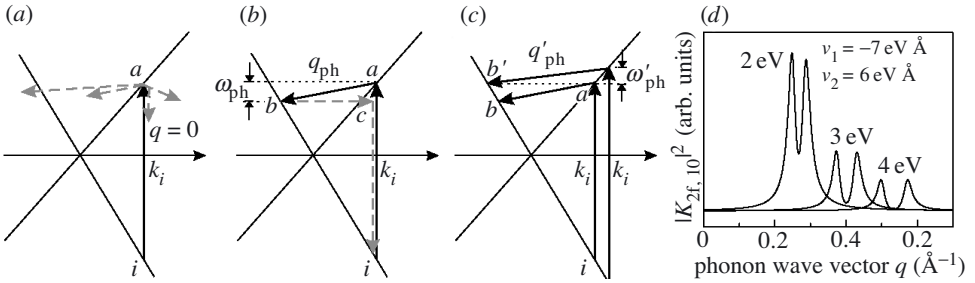

Figure 5. Double-resonant Raman scattering for two linear bands. (*a*) Resonant excitation of an electron–hole pair followed by non-resonant scattering of the electron. (*b*) Double-resonant Raman scattering occurs for one pair $(\omega_{\rm ph}, q_{\rm ph})$ for a given laser energy. (*c*) For a different incoming laser energy the double-resonant condition selects a different $(\omega'_{\rm ph}, q'_{\rm ph})$ pair. Resonant (non-resonant) transitions are indicated by full (dashed) arrows. (*d*) Calculated Raman spectrum for linear electron and phonon dispersion. After Reich *et al.* (2004).

or the observation of the phonon density of states (see Wang *et al.* (1990) for a review of the earlier works). All these attempts failed, however, to explain the excitation-energy dependence of the peaks, which, in the first-order Raman spectrum, is most pronounced for the D mode. Thomsen & Reich (2000) showed that this peculiar behaviour is due to a double-resonant Raman process that selectively enhances a particular phonon wave vector and hence phonon frequency. We first present a text-book example of double-resonant Raman scattering before we turn more specifically to the situation in graphite.

(*a*) *Linear bands*

Consider two linear electronic bands that cross at the Fermi energy as shown in figure 5. For such an electronic band structure an incoming photon of energy E_1 can always excite a resonant transition from a state i in the valence band to a state a in the conduction band with $E_1 = E_a^{\rm e} - E_i^{\rm e} = E_{ai}^{\rm e}$, where E_i and E_a are the eigenenergies of the electrons. The excited electron can be scattered by phonons of arbitrary wave vector q as shown in figure 5*a* by the dashed arrows. The scattering probability, however, will be particularly high if the phonon scatters the electron from the real electronic states a into another real state b. For a given phonon and electron dispersion this condition (both a and b are among the allowed electronic states) is only fulfilled by one pair of phonon energy $\omega_{\rm ph}$ and phonon wave vector $q_{\rm ph}$. It is important to understand that the non-resonant scattering by phonons as in figure 5*a* actually takes place; it is not forbidden by selection rules. The resonant transition mediated by a phonon in figure 5*b* is, however, by far the most dominant and the corresponding $(\omega_{\rm ph}, q_{\rm ph})$ pair is selectively enhanced by the large scattering cross-section (Baranov *et al.* 1988; Martin & Falicov 1983; Sood *et al.* 2001; Thomsen & Reich 2000).

For a Raman process the linear momentum has to be conserved, because the momentum of the light is small when compared with the Brillouin zone. This is where the defect comes into the picture; it scatters the electron back elastically k_i (dashed arrow from state b to state c in figure 5*b*). Finally, the electron–hole pair recombines, emitting the scattered photon $E_2 = E_1 - \hbar\omega_{\rm ph}$. In figure 5*a*, *b*, resonant transitions are indicated by full arrows, non-resonant transitions by dashed arrows.

The process in figure 5*b* involves two resonances; it is therefore called double-resonant Raman scattering.

The Raman spectra for defect-induced scattering can be calculated by evaluating the Raman cross-section $K_{2\mathrm{f},10}$ (Cardona 1982; Martin & Falicov 1983)

$$K_{2\mathrm{f},10} = \sum_{a,b,c} \frac{\mathcal{M}_{\mathrm{eR},\rho}\mathcal{M}_{\mathrm{e-def}}\mathcal{M}_{\mathrm{ep}}\mathcal{M}_{\mathrm{eR},\sigma}}{(E_1 - E^{\mathrm{e}}_{ai} - \mathrm{i}\gamma)(E_1 - \hbar\omega_{\mathrm{ph}} - E^{\mathrm{e}}_{bi} - \mathrm{i}\gamma)(E_1 - \hbar\omega_{\mathrm{ph}} - E^{\mathrm{e}}_{ci} - \mathrm{i}\gamma)} + \sum_{a,b,c} \frac{\mathcal{M}_{\mathrm{eR},\rho}\mathcal{M}_{\mathrm{ep}}\mathcal{M}_{\mathrm{e-def}}\mathcal{M}_{\mathrm{eR},\sigma}}{(E_1 - E^{\mathrm{e}}_{ai} - \mathrm{i}\gamma)(E_1 - E^{\mathrm{e}}_{bi} - \mathrm{i}\gamma)(E_1 - \hbar\omega_{\mathrm{ph}} - E^{\mathrm{e}}_{ci} - \mathrm{i}\gamma)}, \quad (4.1)$$

where the sum runs over all intermediate states a, b and c. $\mathcal{M}_{\mathrm{eR}}$ are the matrix elements for the optical transitions, $\mathcal{M}_{\mathrm{ep}}$ for electron–phonon interactions and $\mathcal{M}_{\mathrm{e-def}}$ for the elastic scattering of the carriers by the defect. γ accounts for the finite lifetime of the excited states; the energies in the denominator were introduced above. The first term in equation (4.1) corresponds to the time order in figure 5; the second term describes the processes where the electron is first scattered by a defect and then by a phonon. All other time orders do not yield resonant transitions and can, therefore, safely be neglected. Note that equation (4.1) is more general than figure 5; it contains incoming as well as outgoing resonances, non-resonant or only single-resonant transitions, and also scattering by holes instead of electrons.

Thomsen & Reich (2000) showed that for the example of linear bands the Raman cross-section can be calculated analytically. For simplicity we restrict ourselves to the first term in the Raman cross-section, which yields

$$K_{2\mathrm{f},10} = C\frac{\mathcal{M}_{\mathrm{eR},\rho}\mathcal{M}_{\mathrm{e-def}}\mathcal{M}_{\mathrm{ep}}\mathcal{M}_{\mathrm{eR},\sigma}}{(\kappa_2 - qv_2/(v_2 - v_1))(\kappa_2 + qv_1/(v_2 - v_1))}, \quad (4.2)$$

where

$$C = \ln \kappa_2/\kappa_1 \frac{2\kappa_2 - q}{(v_2 - v_1)^2\hbar\omega_{\mathrm{ph}}}$$

is a slowly varying function of q,

$$\kappa_1 = \frac{E_1 - \mathrm{i}\hbar\gamma}{v_2 - v_1} \quad \text{and} \quad \kappa_2 = \frac{E_1 - \hbar\omega_{\mathrm{ph}} - \mathrm{i}\hbar\gamma}{v_2 - v_1},$$

and v_1 and v_2 are the Fermi velocities. In figure 5*d* we plot the calculated Raman spectrum, which is proportional to $|K_{2\mathrm{f},10}|^2$, for linear electronic bands and a phonon dispersion that is linear as well ($\gamma = 0.1$ eV, see the figure for v_1 and v_2). For a given laser energy two peaks appear in the spectra. For these q the double-resonance condition is fulfilled. They correspond to the phonon wave vectors where one of the denominators in equation (4.2) vanishes, i.e.

$$q = \frac{E_1 - \hbar\omega_{\mathrm{ph}}(q)}{v_2} \quad \text{and} \quad q = \frac{E_1 - \hbar\omega_{\mathrm{ph}}(q)}{-v_1}. \quad (4.3)$$

When increasing the laser energy the double-resonant q shift to larger values. This is easily understood by the illustration in figure 5*c*, which shows the double-resonant process for two slightly different laser energies. Since the energy and the momentum of the photo-excited electron are larger for increasing E_1, the double-resonant phonon

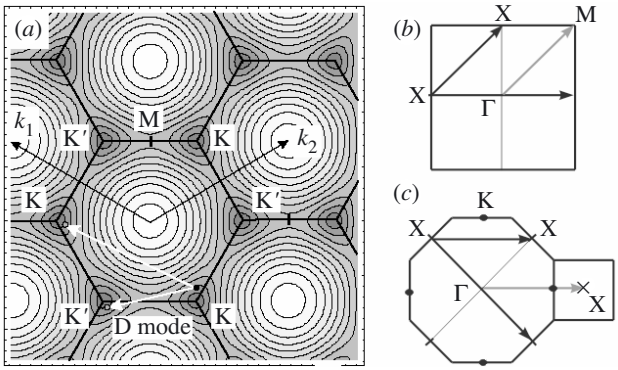

Figure 6. (*a*) Brillouin zone and contour plot of the π^* band of graphene. The arrows indicate the two possible double-resonant transitions. The phonon wave vectors are close to the K or the Γ point of the Brillouin zone. Cuts through the Brillouin zones of (*b*) the simple tetragonal and (*c*) the face-centred cubic (FCC) lattices. In the tetragonal Brillouin zone an electron at X can be scattered resonantly by an M- or a Γ-point phonon; in the FCC case either Γ- or X-point phonons yield symmetry-imposed resonances.

wave vector increases as well. In turn the phonon frequency changes to higher energies because we assumed a monotonically increasing dispersion for the phonon branch. The absolute values of the phonon wave vectors in figure 5*d* are comparable with the typical extensions of the Brillouin zone of a crystal (1.26 Å^{-1} for a lattice constant of 2.5 Å). Double-resonant Raman scattering can thus probe the phonon dispersion far away from the Γ point.

From equation (4.3) we can derive a general approximation for the double-resonant wave vectors. Neglecting the phonon energies in equation (4.3) and assuming the two Fermi velocities to be the same, $v_1 = v_2 = v$, equation (4.3) simplifies with $E_1 = 2vk_e$ to $q \approx 2k_e$, where k_e is the wave vector of the photo-excited carriers. This relationship can also be seen in figure 5*b*. The $q \approx 2k_e$ approximation, often called a 'selection rule', is very useful for quickly finding the double-resonant phonon wave vector for a given excitation energy. We will use it later to map the disorder-induced frequencies onto the Brillouin zone of graphite and thus to find the phonon dispersion from double-resonant Raman scattering.

(*b*) *Graphite*

From the textbook example we saw that double resonances in Raman scattering are given by a convolution of the electronic band structure and the phonon dispersion. To describe defect-induced Raman processes in graphite we need to know the electronic states for optical transitions in the visible (up to *ca.* 3 eV). Only the π electrons have eigenstates with energies close to the Fermi level E_F; the π and π^* bands cross at the six K and K′ points of the Brillouin zone (Wallace 1947). The bands around the K points can be very well approximated by a linear dispersion and correspond to the example of the last section.

Figure 6*a* shows a contour plot of the π^* conduction band in the Brillouin zone of graphene (Reich *et al.* 2002; Saito *et al.* 1998; Wallace 1947). An electron (black circle) was resonantly excited into the conduction band in the first step of the Raman process. Let us for simplicity assume that the phonon energy corresponds exactly to

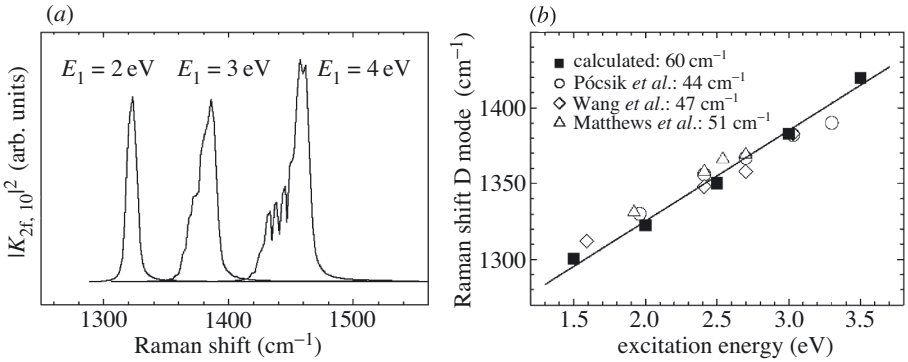

Figure 7. (*a*) Calculated Raman spectra for the D mode in graphite for three different laser energies. (*b*) Calculated (full squares) and measured (open symbols) frequencies of the D mode as a function of excitation energy. From Thomsen & Reich (2000); the measurements were taken from Wang *et al.* (1990), Pócsik *et al.* (1998) and Matthews *et al.* (1999).

the difference between two energy contours. Which phonon wave vectors then yield a second resonant transition? As we can see by the white arrows in figure 6*a*, there are two distinct possibilities: the phonon can scatter the electron from a state close to K to one of the K′ points, or from K to another K point. The first process requires a phonon wave vector close to the K point of graphene and gives rise to the D mode in graphite. Scattering from K to K occurs by phonons with $\boldsymbol{q} \approx \boldsymbol{k}_1 = \boldsymbol{0}$, i.e. close to the Γ point of the Brillouin zone. If we neglect the phonon energy, the selection of the double-resonant wave vector is entirely given by the symmetry in reciprocal space. The band structure of graphene is the same at all K and K′ points because they are connected by reciprocal lattice vectors and time inversion.

To see the selection of the double-resonant wave vector by the symmetry in reciprocal space more clearly, we show two other examples in figure 6*b*, *c*. In a simple tetragonal lattice (figure 6*b*) an electron at the X point is scattered to a symmetry-equivalent state either by a Γ- or an M-point phonon. In the diamond lattice X- or Γ-point vibrations yield scattering from one X point to another X point of the Brillouin zone (see figure 6*c*).

Let us now return to the situation in graphite and, in particular, to the D mode. Thomsen & Reich (2000) first calculated the Raman spectra of the D mode using the concept of double resonances. Their results are reproduced in figure 7*a*, which illustrates nicely that a Raman line appears by defect-induced resonances and shifts to higher frequencies under increasing excitation energy. Figure 7*b* compares the experimental and theoretical frequencies. The agreement is found to be excellent, showing that double-resonant Raman scattering explains the curious excitation-energy dependence of the defect-induced Raman modes in graphite. As we discuss below, the other peculiarities of the graphite Raman spectrum can also be understood by double-resonant scattering. The D* mode is an overtone of the D peak where the electron is backscattered by a second phonon instead of a defect. The differences between Stokes and anti-Stokes scattering arise because the double-resonant condition is slightly different for the creation and destruction of a phonon.

There is an alternative approach to explaining the appearance of the D mode and its excitation-energy dependence. It is based on the lattice dynamics of small

aromatic molecules and their Raman spectra (Castiglioni *et al.* 2001; Mapelli *et al.* 1999). In these molecules, which can be viewed as small graphitic flakes, the D mode has a Raman-active eigenvector; its frequency depends on the actual size and shape of the molecule in question. The shift with excitation energy results from a resonant selection of a particular molecule by the incoming laser. For defect scattering induced by the small size of the graphitic microcrystals, the solid-state approach presented above and the molecular approach can be shown to be the same. The latter fails, however, to explain the D^* mode and its properties in perfect graphite. On the other hand, it has been argued (Ferrari & Robertson 2001) that double-resonant Raman scattering cannot explain why only one phonon branch shows strong double resonances. The other defect-induced peaks are much weaker than the D mode. To understand the selectivity of the process we have to look at the matrix elements in the Raman cross-section.

(*c*) *Selection rules*

In this section we first derive the symmetry-imposed selection rules for double-resonant Raman scattering. The symmetries of the electronic states and the phonon branches along high-symmetry lines impose strict rules on which phonons give rise to a double-resonant Raman signal. In particular, the highest Raman intensity is expected for TO phonons close to the K point of the Brillouin zone, whereas out-of-plane modes cannot participate in double resonances. We then discuss *ab initio* calculations of the electron–phonon coupling in graphite that were performed recently (Piscanec *et al.* 2004).

Figure 8 shows the electronic π and π^* band structure of graphene along the MK′ΓKM line (Reich *et al.* 2002). The electronic states are labelled by their irreducible representations. Optical transitions from the valence to the conduction band (first resonance from the open to the closed circles) are induced by the Γ_6^- representation, i.e. in plane-polarized light. For the excited electron there are two possibilities for scattering resonantly to another state by emitting a phonon: scattering within the same band across the Γ point or scattering across K into another band. The apparent third possibility, scattering across Γ and K′, vanishes by destructive interference in the summation over all intermediate states (see Martin & Falicov (1983) and Martin (1974) for details).

Scattering within the same band across Γ requires a phonon wave vector close to $2(\boldsymbol{k}_1 - \boldsymbol{k}_2)/3$ or equivalent points in the Brillouin zone, i.e. close to the K points. Only totally symmetric modes can resonantly couple electrons within the same non-degenerate band. For scattering across the K point, in contrast, the necessary wave vectors are comparatively small and the phonon has to belong to the T_3 representation. For the electron–phonon matrix element to be non-vanishing the double-resonant phonon thus has to be of T_1 (A_1) symmetry close to K and of T_3 (B_1) symmetry close to Γ. Before discussing which phonon branches meet the outlined requirements, let us consider the third step in the Raman process, the elastic backscattering by a defect. For defects coupling states of the same symmetry, the matrix element $\mathcal{M}_{\mathrm{e\text{–}def}}$ is expected to be large. Moreover, the virtual electronic state after defect scattering (state *c* in figure 5*c*) is very close to an allowed electronic state of the same symmetry. The third denominator in the Raman cross-section in equation (4.1) is, therefore, of the same order as the phonon energy *ca.* 0.2 eV. In

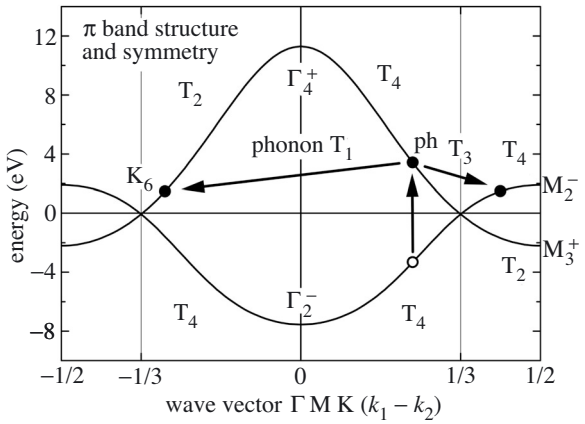

Figure 8. Electronic band structure and symmetry of the π and π^* states in graphene along the ΓKM line. The possible phonon species leading to a double-resonant transition are T_1 (A_1 in molecular notation) for scattering across the Γ point and T_3 (B_1) for scattering across K.

contrast, for backscattering from the T_4 band either electrons of different symmetry have to be coupled (small $\mathcal{M}_{\text{e–def}}$) or the closest allowed electronic states of the same symmetry is *ca.* 2 eV away. Although scattering across the K point yields double resonances, the overall Raman intensity is expected to be weaker than for KK′ scattering because of the symmetry-imposed selection rules.

Along ΓK the TO and the LA branches belong to T_1 and the LO and the TA branches to T_3; the out-of-plane modes belong to T_2 and T_4; they cannot induce double resonances for graphene. The TO and LA branches thus meet the requirement for double-resonant scattering close to K. The matrix element for electron–phonon coupling is expected to be much stronger for the TO than the LA phonon because the TO phonon, in contrast to the LA phonon, (i) is Raman active at the Γ point and (ii) can couple electronic states exactly at the K and K′ points of the Brillouin zone. Thus, the TO phonon is the candidate for the strongest double-resonant Raman signal and the origin of the D mode. As pointed out by Ferrari & Robertson (2000, 2001), the LO branch was incorrectly assigned to the D band by Thomsen & Reich (2000) and in other papers (Kürti *et al.* 2002; Matthews *et al.* 1999; Pócsik *et al.* 1998; Saito *et al.* 2002). The assignment of the TO branch to the D band is consistent with the calculations for aromatic molecules (Castiglioni *et al.* 2001) and the phonon dispersion of graphite from inelastic X-ray scattering (Maultzsch *et al.* 2004). Close to the Γ point the LO and TA branches can induce double resonances. TA scattering will be negligible compared with LO scattering due to the small electron–phonon coupling of the acoustic mode at small q. The discussion presented so far is strictly valid only for graphene. When including the coupling between the graphene layers, a refined analysis shows that double resonances can also result from LO and TA modes close to K and TO and LA phonons around Γ. However, these are secondary effects that account only for weak disorder signals.

The two most prominent features in the disorder-induced graphite Raman spectrum up to 1600 cm^{-1} are the D mode and a peak around 1620 cm^{-1}, i.e. right above the E_{2g} line, often called G′ (see figures 3*b* and 4*b*). From the symmetry analysis we can assign them to the TO branch close to K and the LO mode close to Γ. The rela-

tive Raman intensities of these two peaks are of the order of $I_{\mathrm{D}}/I_{\mathrm{G}'} \approx 10$. Since the intensity is proportional to the square of the Raman cross-section, this yields a factor of approximately three between their Raman cross-sections. Considering the differences in the vibrational density of states (higher for G′ than for D) and the combined matrix elements (lower for G′ than for D), this ratio is quite reasonable. Piscanec *et al.* (2004) recently calculated the electron–phonon interaction in graphite using first-principles methods. They showed that the matrix element for the LO phonon at K is two orders of magnitude weaker than for the TO-derived phonon, which nicely confirms the symmetry arguments. For the intensity ratio between the D and G′ line they obtained $I_{\mathrm{D}}/I_{\mathrm{G}'} \approx 2.5$; the additional factor of four when compared with experiment most likely arises from the elastic scattering process. The symmetry of the TO and LO branches at K and Γ, respectively, combined with the peculiar Fermi surface of graphene, give rise to a singular behaviour of the phonon dispersion at the two high-symmetry points (Piscanec *et al.* 2004). This behaviour, known as a Kohn anomaly, explains the strong electron–phonon coupling in graphite as well as the large slope of the disorder-induced D Raman peak; details are discussed in another article in this issue. The other, weaker, disorder-induced lines in the Raman spectrum of graphite can also be assigned to phonon branches and used to measure the phonon dispersion of graphite. Before we do so, however, let us turn to the second-order spectrum and Stokes and anti-Stokes scattering in this material.

(*d*) *Second-order Raman spectrum*

The second-order Raman spectrum of graphite corresponds to the overtones and combinations of the disorder-induced bands. It results from double-resonant Raman scattering by two phonons instead of a phonon and a defect. The double resonances explain why the second-order signal in graphite and similar materials is so strong when compared with the Raman-active $\mathrm{E}_{2\mathrm{g}}$ phonon. Two phonon processes with $q \neq 0$ are allowed in perfect graphite crystals as well as in the presence of defects. Therefore, the second-order signal is the same in parts (*a*) and (*b*) of figure 3. Extending the symmetry analysis of the previous section to overtone scattering we find that double resonances by two phonons are expected if the two modes belong to branches of the same symmetry, i.e. overtones and the combinations LO + TA and TO + LA. An assignment of the second-order bands will be performed in § 5.

(*e*) *Anti-Stokes scattering*

In figure 4*c* we presented measurements by Tan *et al.* (1998) showing that the Stokes and anti-Stokes frequencies are different for the D mode in graphite by $\Delta\hbar\omega = 7\,\mathrm{cm}^{-1}$. When double resonances were discovered as the origin of the D band Thomsen & Reich (2000) pointed out that the resonance conditions differ for the creation and destruction of a phonon. The double-resonance process shown in figure 5*b* is for Stokes scattering. We obtain an anti-Stokes process by inverting all arrows in the picture. This process is also double resonant, but with a different time order, an outgoing instead of an incoming resonance and, most importantly, at a different excitation energy (Tan *et al.* 2002; Zólyomi & Kürti 2002). In general, the Raman cross-section for Stokes scattering K_{S} is exactly the same as the cross-section for anti-Stokes scattering K_{aS} if we interchange the incoming and outgoing photon

(time inversion), i.e.

$$K_{aS}[E_2, \hbar\omega_{aS}(E_1), E_1] = K_{\mathrm{S}}[E_1, \hbar\omega_{\mathrm{S}}(E_2), E_2] = K_{\mathrm{S}}[E_1, \hbar\omega_{\mathrm{S}}(E_2), E_1 + \hbar\omega_{aS}(E_1)]. \tag{4.4}$$

In other words $\hbar\omega_{aS}(E_1) = \hbar\omega_{\mathrm{S}}(E_2)$. Since we know the dependence of the Stokes frequency on excitation energy we can calculate the frequency difference

$$\Delta\hbar\omega = \hbar\omega_{aS}(E_1) - \hbar\omega_{\mathrm{S}}(E_1) = \frac{\partial\hbar\omega_{\mathrm{S}}}{\partial E}\hbar\omega_{aS}(E_1). \tag{4.5}$$

Tan *et al.* (1998) measured an anti-Stokes frequency of $1379\,\mathrm{cm}^{-1}$ and a D mode slope of $43\,\mathrm{cm}^{-1}\,\mathrm{eV}^{-1}$. The expected $\Delta\hbar\omega = 7.4\,\mathrm{cm}^{-1}$ is in excellent agreement with the reported value ($7\,\mathrm{cm}^{-1}$; see figure 4*c*). As discussed by Zólyomi & Kürti (2002) and Tan *et al.* (2002) the frequency difference for the D* overtone is predicted to be four times larger than for the D mode, because both the energy differences between E_1 and E_2 and the slope of the Raman peak with laser energy are doubled. This also agrees very well with the experimentally reported differences. In turn, equation (4.5) can be used to determine, at least approximately, the slope of a disorder band. The experimental advantage of this procedure when compared with measuring the frequency for two different excitation energies is that no change in laser frequency is necessary.

5. Phonon dispersion from double-resonant Raman scattering

The change in phonon frequency with excitation energy is the fingerprint of a double resonance. The shift is caused by the dispersion of the phonon branches with varying phonon wave vector. Thus, the observed phonon frequency can be used to measure the phonon dispersion of a material. This idea was first applied to graphite by Saito *et al.* (2002). The problem of the approach is that the double-resonant phonon wave vector depends on the phonon dispersion as can be seen in the linear bands example (equation (4.3)). Nevertheless, we will see that with some approximations good agreement is found between the measured disorder-induced frequencies and the phonon dispersion obtained by other methods.

To find the double-resonant q we assume that the $q = 2k_{\mathrm{e}}$ rule is strictly valid, i.e. we drop the $\hbar\omega_{\mathrm{ph}}(q)$ dependence in equation (4.3). For finding the electron (or hole) wave vector we look at the electronic transition energies along Γ–K and K–M. Either the first (incoming resonance) or the last (outgoing) step in the Raman process has to correspond to a real electronic transition of graphite. For the calculation of the electronic energies we used the third-order tight-binding formalism worked out by Reich *et al.* (2002). We further assume that the phonon wave vector has to be along the Γ–K or K–M symmetry lines. The last approximation is not so rough as it first seems because of the sixfold symmetry of the graphite lattice. The double-resonant phonon wave vector q for scattering within the same band (approximately K-point phonons) is $2k_{\mathrm{e}}$, whereas the q for scattering between the two high-symmetry directions (approximately Γ-point phonons) is the difference between k_{e}(ΓK) and k_{e}(KM). We included the asymmetry between ΓK and KM (trigonal warping), because we found that for energies in the visible k_{e} differs by 20–30% on the two sides of K.

Figure 9*a* shows the measured disorder-induced phonon frequencies mapped onto the graphite Brillouin zone (grey dots); figure 9*b* is the same but for the second-order bands. The experimental data were taken from a variety of published measurements (see figure caption for details). The black lines are *ab initio* calculations

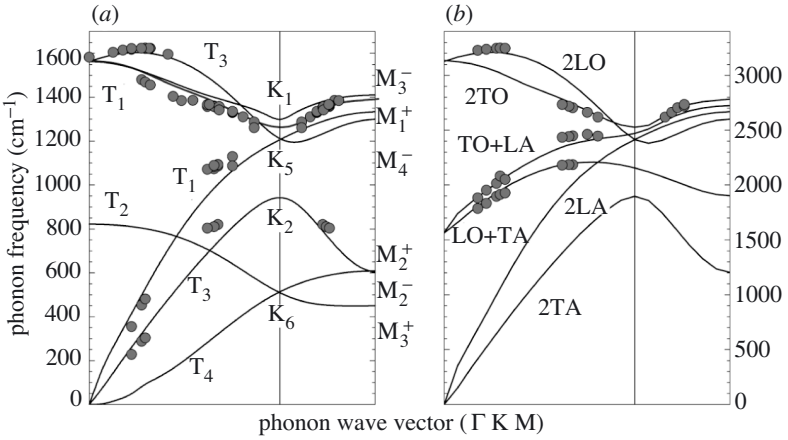

Figure 9. Phonon dispersion of graphite by double-resonant Raman scattering. (*a*) Frequency of the disorder-induced modes mapped onto the graphite Brillouin zone as described in the text (grey dots). Some of the data were measured by us; the others were taken from Wang *et al.* (1990), Pócsik *et al.* (1998), Kawashima & Katagiri (1995) and Tan *et al.* (2001, 2002). Black lines are *ab initio* calculations of the lattice dynamics of graphene; the grey line is a cubic spline interpolation of the TO branch measured by Maultzsch *et al.* (2004). (*b*) Second-order bands of graphite mapped onto the Brillouin zone; data from Kawashima & Katagiri (1995) and Tan *et al.* (2001, 2002). Lines are the sum of the overtones of the phonon branches in (*a*) and those combinations which yield the totally symmetric representation. No assignment was obtained for the second-order mode at *ca.* 2900 cm^{-1}; this mode was omitted from the figure.

of the phonon dispersion of graphene by Maultzsch *et al.* (2004). This calculation was found to excellently describe the phonon dispersion measured by inelastic X-ray scattering except for the TO branch. For this branch we therefore included a cubic spline extrapolation of the X-ray data (grey line). The D mode excitation-energy dependence describes very well the TO branch of graphite; a good agreement is also found for the LO branch along ΓK and the second-order features of both modes. The LO Raman data (up to 1625 cm^{-1}) are systematically a little higher than the X-ray measurements (1610 cm^{-1}), a difference that is not understood presently. For the acoustic disorder-induced modes the agreement seems to be less satisfactory at first. Note that in contrast to Saito *et al.* (2002) and Kawashima & Katagiri (2002) we assign the *ca.* 800 cm^{-1} peak to the TA branch of graphite and not to the out-of-plane mode. The vibrations perpendicular to the planes do not participate in double-resonant scattering as discussed in § 4 *c*. This assignment is, moreover, consistent with the weak LO + TA overtone at 2180 cm^{-1} observed by Kawashima & Katagiri (1995) (see figure 9*b*).

The less good agreement for the acoustic branches is, at least partly, a consequence of their much stronger dispersion and our neglecting the phonon term in the double-resonant condition. For the acoustic phonons between Γ and K but close to K the phonon term shifts the double-resonant q to larger values and to smaller values for q close to Γ (Cancado *et al.* 2002). The magnitude of the q shift increases with the slope of the phonon dispersion and with the phonon energy. This is in good qualitative agreement with the discrepancies in figure 9; we will, however, not attempt to correct for this effect within the present paper.

From figure 9*a* it is obvious that the most complete set of data is available for the TO branch of graphite. This is due to the high intensity of the D mode, but also to the many studies with different lasers performed for this mode. The number of data in the other frequency ranges is very limited. Although these disorder-induced bands are weaker in intensity by approximately two orders of magnitude when compared with the D band, they are well within the detection limit of modern Raman set-ups. It would be quite interesting to measure the graphite disorder modes over a wider range of excitation energies. Studies on the second-order features, where a very nice agreement is seen between theory and experiment, are also very promising.

6. Conclusion

In this paper we have reviewed the experimental and theoretical work on the Raman spectra of graphite. Graphite has two Raman-active modes at the Γ point at 44 and 1582 cm^{-1}. In addition to these two phonons, several peaks are observed in the Raman spectra that do not correspond to Γ-point vibrations. The most prominent of these disorder-induced lines are the so-called D mode and its D^* overtones in the second-order spectra. We showed that the disorder modes appear because of a double-resonant Raman process that, for a given laser energy and phonon branch, selectively enhances a particular phonon wave vector and phonon frequency. The double-resonance condition depends strongly on the wave vector of the photo-excited electrons and holes and hence on excitation energy. The fingerprint of a double resonance in Raman scattering is, therefore, the dependence of the phonon frequencies on the incoming laser light. Another typical feature is a frequency difference between Stokes and anti-Stokes scattering.

After introducing the theory of double-resonant Raman scattering with the example of two linear bands and a linear phonon dispersion, we applied the concept to graphite. We worked out the symmetry-imposed selection rules for both the wave vector and the phonon species that participate in the resonant transitions. In particular, we showed that the two strongest features in the disorder spectrum correspond to the TO branch close to K (D mode) and the LO branch around Γ (G'). Finally, we discussed how double resonances can be used to measure the phonon dispersion of a material. For graphite an excellent agreement is found between the double-resonant phonon frequencies and the phonon dispersion known independently from theory and other experiments.

We thank J. Maultzsch for many helpful discussions about double-resonant Raman scattering in graphite and carbon nanotubes and also for her help with the Raman measurements used in figure 9. We are very grateful to S. Morgner for her measurements of the Raman spectra in figure 3. We obtained the rare single crystals of graphite used in the measurement from A. V. Tamashausky. S.R. was supported by the Berlin-Brandenburgische Akademie der Wissenschaften, the Oppenheimer Fund and Newnham College. Parts of this work were supported by the Deutsche Forschungsgemeinschaft under grant number Th 662/8-1.

References

Baranov, A. V., Bekhterev, A. N., Bobovich, Y. S. & Petrov, V. I. 1988 Interpretation of certain characteristics in Raman spectra of graphite and glassy carbon. *Opt. Spectrosc.* **62**, 612.

Cancado, L. G., Pimenta, M. A., Saito, R., Jorio, A., Ladeira, L. O., Grueneis, A., Souza-Filho, A. G., Dresselhaus, G. & Dresselhaus, M. S. 2002 Stokes and anti-Stokes double resonance Raman scattering in two-dimensional graphite. *Phys. Rev.* B **66**, 035415.

Cardona, M. 1982 Resonance phenomena. In *Light scattering in solids. II* (ed. M. Cardona & G. Güntherodt). Topics in Applied Physics, vol. 50, p. 19. Springer.

Castiglioni, C., Negri, F., Rigolio, M. & Zerbi, G. 2001 Raman activation in disordered graphites of the A_1 symmetry forbidden $k \neq 0$ phonon: the origin of the D line. *J. Chem. Phys.* **115**, 3769.

Dubay, O. & Kresse, G. 2003 Accurate density functional calculations for the phonon dispersion relations of graphite layer and carbon nanotubes. *Phys. Rev.* B **67**, 035401.

Ferrari, A. & Robertson, J. 2000 Interpretation of Raman spectra of disordered and amorphous carbon. *Phys. Rev.* B **61**, 14095.

Ferrari, A. & Robertson, J. 2001 Resonant Raman spectroscopy of disordered, amorphous, and diamondlike carbon. *Phys. Rev.* B **64**, 075414.

Grüneis, A., Saito, R., Kimura, T., Cancado, L. G., Pimenta, M. A., Jorio, A., Souza Filho, A. G., Dresselhaus, G. & Dresselhaus, M. S. 2002 Determination of two-dimensional phonon dispersion relation of graphite by Raman spectroscopy. *Phys. Rev.* B **65**, 155405.

Jishi, R. A. & Dresselhaus, G. 1982 Lattice-dynamical model for graphite. *Phys. Rev.* B **26**, 4514.

Kawashima, Y. & Katagiri, G. 1995 Fundamentals, overtones, and combinations in the Raman spectrum of graphite. *Phys. Rev.* B **52**, 10053.

Kawashima, Y. & Katagiri, G. 2002 Evidence for nonplanar atomic arrangement in graphite obtained by Raman spectroscopy. *Phys. Rev.* B **66**, 104109.

Kresse, G., Furthmüller, J. & Hafner, J. 1995 *Ab initio* force constant approach to phonon dispersion relations of diamond and graphite. *Europhys. Lett.* **32**, 729.

Kürti, J., Zólyomi, V., Grüneis, A. & Kuzmany, H. 2002 Double resonant Raman phenomena enhanced by van Hove singularities in single-wall carbon nanotubes. *Phys. Rev.* B **65**, 165433.

Mapelli, C., Castiglioni, C., Zerbi, G. & Müllen, K. 1999 Common force field for graphite and polycyclic aromatic hydrocarbons. *Phys. Rev.* B **60**, 12710.

Martin, R. M. 1974 Resonance Raman scattering near critical points. *Phys. Rev.* B **10**, 2620.

Martin, R. M. & Falicov, L. M. 1983 Resonant Raman scattering. In *Light scattering in solids. I. Introductory concepts* (ed. M. Cardona), 2nd edn. Topics in Applied Physics, vol. 8, p. 79. Springer.

Matthews, M. J., Pimenta, M. A., Dresselhaus, G., Dresselhaus, M. S. & Endo, M. 1999 Origin of dispersive effects of the Raman D band in carbon materials. *Phys. Rev.* B **59**, R6585.

Maultzsch, J., Reich, S., Schlecht, U. & Thomsen, C. 2003 High-energy phonon branches of an individual metallic carbon nanotube. *Phys. Rev. Lett.* **91**, 087402.

Maultzsch, M., Reich, S., Thomsen, C., Requardt, H. & Ordejón, P. 2004 Phonon dispersion of graphite. *Phys. Rev. Lett.* **92**, 075501.

Nemanich, R. J. & Solin, S. A. 1979 First- and second-order Raman scattering from finite-size crystals of graphite. *Phys. Rev.* B **20**, 392.

Pavone, R., Bauer, R., Karch, K., Schütt, O., Vent, S., Windl, W., Strauch, D., Baroni, S. & de Gironcoli, S. 1993 *Ab-initio* phonon calculations in solids. *Physica* B **220**, 439.

Piscanec, S., Lazzeri, M., Mauri, F., Ferrari, A. C. & Robertson, J. 2004 Kohn anomalies and electron–phonon interaction in graphite. (Submitted.) (Available at http://arxiv.org/abs/cond-mat?0407164.)

Pócsik, I., Hundhausen, M., Koos, M. & Ley, L. 1998 Origin of the D peak in the Raman spectrum of microcrystalline graphite. *J. Non-cryst. Solids* **227–230**, 1083.

Reich, S., Maultzsch, J., Thomsen, C. & Ordejón, P. 2002 Tight-binding description of graphene. *Phys. Rev.* B **66**, 035412.

Reich, S., Thomsen, C. & Maultzsch, J. 2004 *Carbon nanotubes: basic concepts and physical properties*. Wiley-VCH.

Rousseau, D. L., Bauman, R. P. & Porto, S. P. S. 1981 Normal mode determination in crystals. *J. Raman Spectrosc.* **10**, 253.

Sánchez-Portal, D., Artacho, E., Soler, J. M., Rubio, A. & Ordejón, P. 1999 *Ab initio* structural, elastic, and vibrational properties of carbon nanotubes. *Phys. Rev.* B **59**, 12678.

Saito, R., Dresselhaus, G. & Dresselhaus, M. S. 1998 *Physical properties of carbon nanotubes*. London: Imperial College Press.

Saito, R., Jorio, A., Souza-Filho, A. G., Dresselhaus, G., Dresselhaus, M. S. & Pimenta, M. A. 2002 Probing phonon dispersion relations of graphite by double resonance Raman scattering. *Phys. Rev. Lett.* **88**, 027401.

Sood, A. K., Gupta, R. & Asher, S. A. 2001 Origin of the unusual dependence of Raman D band on excitation wavelength in graphite-like materials. *J. Appl. Phys.* **90**, 4494.

Tan, P.-H., Deng, Y.-M. & Zhao, Q. 1998 Temperature-dependent Raman spectra and anomalous Raman phenomenon of highly oriented pyrolytic graphite. *Phys. Rev.* B **58**, 5435.

Tan, P., Hu, C., Dong, J., Shen, W. & Zhang, B. 2001 Polarization properties, high-order Raman spectra, and frequency asymmetry between Stokes and anti-Stokes scattering of Raman modes in a graphite whisker. *Phys. Rev.* B **64**, 214301.

Tan, P., An, L., Liu, L., Guo, Z., Czerw, R., Carroll, D. L., Ajayan, P. M., Zhang, N. & Guo, H. 2002 Probing the phonon dispersion relations of graphite from the double-resonance process of Stokes and anti-Stokes Raman scatterings in multiwalled carbon nanotubes. *Phys. Rev.* B **66**, 245410.

Thomsen, C. & Reich, S. 2000 Double-resonant Raman scattering in graphite. *Phys. Rev. Lett.* **85**, 5214.

Tuinstra, F. & Koenig, J. L. 1970 Raman spectrum of graphite. *J. Chem. Phys.* **53**, 1126.

Vidano, R. P., Fischbach, D. B., Willis, L. J. & Loehr, T. M. 1981 Observation of Raman band shifting with excitation wavelength for carbons and graphites. *Solid State Commun.* **39**, 341.

Wallace, P. R. 1947 The band theory of graphite. *Phys. Rev.* **71**, 622.

Wang, Y., Alsmeyer, D. C. & McCreery, R. L. 1990 Raman spectroscopy of carbon materials: structural basis of observed spectra. *Chem. Mater.* **2**, 557.

Wilson, E. B., Decius, J. C. & Cross, P. C. 1980 *Molecular vibrations*. New York: Dover.

Yu, P. Y. & Cardona, M. 1996 *Fundamentals of semiconductors*. Springer.

Zólyomi, V. & Kürti, J. 2002 Calculating the discrepancy between the Stokes and anti-Stokes Raman D band of carbon nanotubes using double resonance theory. *Phys. Rev.* B **66**, 073418.